

Detection of a hot core in the intermediate-mass Class 0 protostar NGC 7129–FIRS 2

A. Fuente¹, R. Neri², and P. Caselli³

¹ Observatorio Astronómico Nacional (IGN), Campus Universitario, Apdo. 112, E-28803 Alcalá de Henares (Madrid), Spain

² Institut de Radioastronomie Millimétrique, 300 rue de la Piscine, 38406 St. Martin d’Hères Cedex, France

³ INAF-Osservatorio Astrofisico di Arcetri, Largo Enrico Fermi 5, I-50125 Firenze, Italy

the date of receipt and acceptance should be inserted later

Abstract. We report high angular resolution (HPBW $\sim 0.6'' \times 0.5''$ at 1.3mm) observations of the Class 0 intermediate-mass (IM) protostar NGC 7129–FIRS 2 using the Plateau de Bure Interferometer. Our observations show the existence of an intense unresolved source in the continuum at 1.3mm and 3mm at the position of the Class 0 object. In addition, compact CH₃CN emission is detected at this position. The high rotational temperature derived from the CH₃CN lines ($T_{rot} \approx 50$ K) as well as the enhanced CH₃CN fractional abundance ($X(\text{CH}_3\text{CN}) \sim 7.0 \cdot 10^{-9}$) show the existence of a hot core in this IM young stellar object. This is, up to our knowledge, the first IM hot core detected so far. Interferometric maps of the region in the CH₃OH $5_{kk'} \rightarrow 4_{kk'}$, and D₂CO $4_{04} \rightarrow 3_{03}$ lines are also presented in this paper. The methanol emission presents two condensations, one associated with the hot core which is very intense in the high upper state energy lines ($E_u > 100$ K) and other associated with the bipolar outflow which dominates the emission in the low excitation lines. Enhanced CH₃OH abundances ($X(\text{CH}_3\text{OH}) \sim 3 \cdot 10^{-8}$ – a few 10^{-7}) are measured in both components. While intense D₂CO $4_{04} \rightarrow 3_{03}$ emission is detected towards the hot core, the N₂D⁺ $3 \rightarrow 2$ line has not been detected in our interferometric observations. The different behaviors of D₂CO and N₂D⁺ emissions suggest different formation mechanisms for the two species and different deuteration processes for H₂CO and N₂H⁺ (surface and gas-phase chemistry, respectively). Finally, the spectrum of the large bandwidth correlator show a forest of lines at the hot core position revealing that this object is extraordinarily rich in complex molecules. To have a deeper insight into the chemistry of complex molecules, we have compared the fractional abundances of the complex O- and N- bearing species in FIRS 2 with those in hot corinos and massive hot cores. Within the large uncertainty involved in fractional abundance estimates towards hot cores, we do not detect any variation of the relative abundances of O- and N-bearing molecules ($[\text{CH}_3\text{CN}]/[\text{CH}_3\text{OH}]$) with the hot core luminosity. However, the O-bearing species H₂CO and HCOOH seem to be more abundant in low and intermediate mass stars than in massive star forming regions. We propose that this could be the consequence of a different grain mantle composition in low and massive star forming regions.

Key words. Stars: formation – individual: NGC7129 – FIRS 2–ISM: abundances – clouds – individual: NGC 7129

1. Introduction

Hot cores are compact objects near or around protostars characterized by warm temperatures ($T_k > 100$ K) and high densities ($n > 10^6 \text{ cm}^{-3}$). These regions are also characterized by a very rich chemistry in complex molecules (CH₃OH, CH₃CN, CH₃OCHO, CH₃OCH₃, C₂H₅CN ...). Hot cores are thought to be associated with high-mass protostars ($M \geq 8 M_\odot$) and to represent an important phase in their evolution toward ultracompact and compact HII regions. Recently, regions characterized by warm temperatures and high densities have also been detected in two low-mass protostars IRAS 16293–

2422 (Ceccarelli et al. 2000; Cazaux et al. 2003) and NGC 1333 IRAS 4A (Bottinelli et al. 2004). Complex molecules typical of hot cores (e.g. HCOOH, CH₃OCHO, CH₃CN, C₂H₅CN) have also been detected in these objects. However, the amount of warm material involved, as well as the chemistry, are different in the two classes of objects. For this reason, the warm regions in the inner envelope of low mass protostars are usually referred to as “hot corinos”.

The formation of complex molecules in hot cores and corinos is poorly understood. In the standard scheme, neutral molecules (CO, CS...) are frozen onto dust grains during the cold pre-stellar phase. If the dust temperature is sufficiently low during this phase, surface hydro-

Send offprint requests to: A. Fuente, e-mail: a.fuente@oan.es

generation of CO leads to the formation of solid H_2CO and CH_3OH (e.g. Brown et al. 1988; Charnley et al. 1992; Caselli et al. 1993). Once the star starts heating the grain surfaces, these molecules (called “parent” species) evaporate, enlarging their abundances in the gas phase. Because of the high temperature and density of hot cores and corinos, these molecules undergo fast neutral-neutral and ion-neutral reactions producing at early stages ($\sim 10^4$ yr) a second generation of complex O-bearing species called “daughter” molecules, such as methyl formate, CH_3OCHO . However, Horn et al. (2004) recently found that the gas-phase reaction sequence between protonated methanol and formaldehyde, crucial for the gas-phase formation of methyl formate, does not proceed in their laboratory experiments. This suggests that surface chemistry is probably playing a key role also in the formation of this species.

Regarding complex N-bearing species (e.g. CH_3CN , $\text{CH}_3\text{CH}_2\text{CN}$), they are observed in hot cores and hot corinos. In the chemical scheme of Rodgers & Charnley (2001), complex N-bearing species are thought to be formed in the gas phase about 10^5 yr after the grain mantle evaporation, only if the gas temperature is sufficiently large (≥ 300 K). On the other hand, Caselli et al. (1993) found that large abundances of ethyl cyanide ($X(\text{CH}_3\text{CH}_2\text{CN}) \sim 10^{-7}$, w.r.t. H_2) can be obtained on grain surfaces, if the dust temperature during the protostellar accreting is around 40 K. In the case of lower temperatures (10–20 K), the $\text{CH}_3\text{CH}_2\text{CN}$ can still be formed on the surface, but with reduced abundances ($\sim 10^{-9}$). Thus, Caselli et al. (1993) suggests that saturated (or H-rich) complex N-bearing species (such as ethyl cyanide) are “parent” species and that they should be observable as soon as the grain mantles are released in the gas phase upon stellar heating of the dust. Later on, “H-poor” N-bearing molecules (e.g. vinyl cyanide, CH_2CHCN) can be formed in the gas phase from the destruction of $\text{CH}_3\text{CH}_2\text{CN}$.

Indeed, if complex species in general are not formed on grain surfaces, there are important problems for understanding the chemical composition of hot corinos: the timescale necessary to convert “parent” molecules into complex “daughter” molecules is much longer than the transit time of the gas in hot corinos (a few hundred years). Therefore, it seems that the chemistry of complex molecules must begin on grain surfaces (at least in hot corinos). However, chemists are still far from a unique interpretation of the hot core (and corino) chemistry. More observational work is needed. In particular, given the large sensitivity of surface and gas-phase chemistry on dust temperature and gas density, it will be extremely important to measure possible variations of complex molecule abundances with the physical characteristics of hot cores, which of course depend on the mass and luminosity of the associated protostar.

In this paper, we present an interferometric study of the hot core associated with the Class 0 IM protostar NGC 7129–FIRS 2. With a luminosity $\sim 500 L_\odot$ and a mass $\sim 5 M_\odot$, FIRS 2 is very likely the youngest IM ob-

ject known at present (Fuente et al. 1998, 2002). An energetic bipolar molecular outflow with a quadrupolar morphology is associated with it (Fuente et al. 2001, hereafter Paper I). Interferometric observations in the continuum at 1mm and the ^{12}CO 2→1 line shows that the quadrupolar morphology of the outflow is due to the superposition of two bipolar molecular outflows FIRS 2-out 1 and FIRS 2-out 2. FIRS 2-out 1 is associated with the Class 0 protostar detected as an intense millimeter clump in the continuum image (MM1 in the nomenclature of Paper I) while FIRS 2-out 2 is associated with a more evolved infrared star (FIRS 2 - IR) undetected at millimeter wavelengths.

A quite complete chemical study of this Class 0 IM source has been carried out by Fuente et al. (2005) (hereafter Paper II) using the 30m IRAM telescope. They detected warm CH_3CN ($T_k > 63$ K) towards the central position which constitutes a strong evidence for the existence of a hot core in this Class 0 IM object. However, the limited angular resolution of these observations make it very difficult to discern between the hot core emission and those of the outflow and/or the warm envelope. The new results presented in this paper confirm the existence of the hot core associated with FIRS 2 and give a first glance of the chemistry of this object. Up to our knowledge, FIRS 2 is the first IM hot core detected thus far. The intermediate kinetic temperature and mass of the FIRS 2 hot core are expected to produce a differentiated chemistry and to furnish a link between the low mass and high mass regimes.

2. Observations

The observations presented in this paper correspond to two different observational projects carried out with the Plateau de Bure interferometer (PdBI). The main set of data was observed on March 08, 2003. The observations were carried out with excellent weather conditions and counts 5 hr of integration time (on-source) with 6-element array in the A configuration which provides the highest angular resolution. The spectral correlator setup was adjusted to observe the CH_3CN 5→4 line with two contiguous 20 MHz units, N_2D^+ 3→2 and D_2CO 4₀₄→3₀₃ with two separated 20 MHz units and the remaining units were configured for maximum continuum sensitivity (see Table 1). These observations show on average system temperatures of 140 K (3mm) and 250 K (1mm), a mean atmospheric water vapour content of 1-2mm, and were made under seeing conditions of 0.3 arcsec. The RF calibrator was 0420-0414, the phase calibrators ordered by right ascension were 1928+738, 2146+608 and 2309+454, and the flux calibrator was MWC 349. The precision in the flux densities is better than 20% at 1mm and better than 10% at 3mm. Images have been created in natural weighting.

In addition, we present the CH_3OH J=5_k→4_k image observed within a previous project in November and December, 1998. The data corresponding to this project were partially published in Paper I. Details about the observations are given in Table 1 and Paper I.

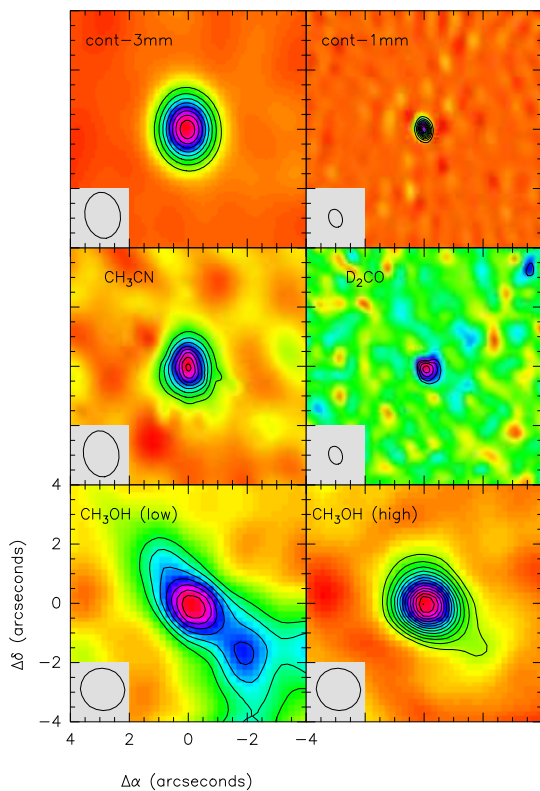


Fig. 1. Interferometric maps of the Class 0 protostar NGC 7129–FIRS 2 in the continuum at 1mm and 3mm, and the following molecular lines: CH₃CN 5→4, D₂CO 4₀₄→3₀₃, CH₃OH 5_{1,4}→4_{1,4}. The panel marked with “CH₃OH (high)” show the integrated intensity map of the lines 5_{3,1}→4_{3,1}, 5_{3,2}→4_{3,2}, 5_{2,2}→4_{2,2} and 5_{3,3}→4_{3,3}. Contour levels are: a) 10 to 60 by 5 mJy/beam; b) 20 to 160 by 20 mJy/beam; c) 0.6 to 2.7 by 0.3 Jy/beam km s⁻¹; d) 0.3 to 0.6 by 0.1 Jy/beam km s⁻¹; e) 1 to 4 by 0.5 Jy/beam km s⁻¹; f) 1 to 7.5 by 0.5 Jy/beam km s⁻¹.

3. Continuum data

The continuum images at 3mm and 1.3mm are shown in Fig. 1. The angular resolution of these images is 3 times better than that of the images previously published in Paper I. Both images show an intense and compact source located at RA(2000)=21:43:01.684, Dec(2000)=66:03:23.619, the position named MM1 in Paper I. There is no indication of the presence of the second and more extended source MM2 which is very likely resolved out in the high angular resolution image.

We have modeled the visibilities to have a deeper insight into the source structure. In Fig. 2 we show the 92 GHz and 230 GHz visibilities vs projected baselines in units of wavelength. The 92 GHz visibilities scaled by a factor of 10.5 match perfectly the 230 GHz visibilities. This suggests that both emissions are arising exactly in the same region. The spectral index is $\alpha=2.56$. The fact

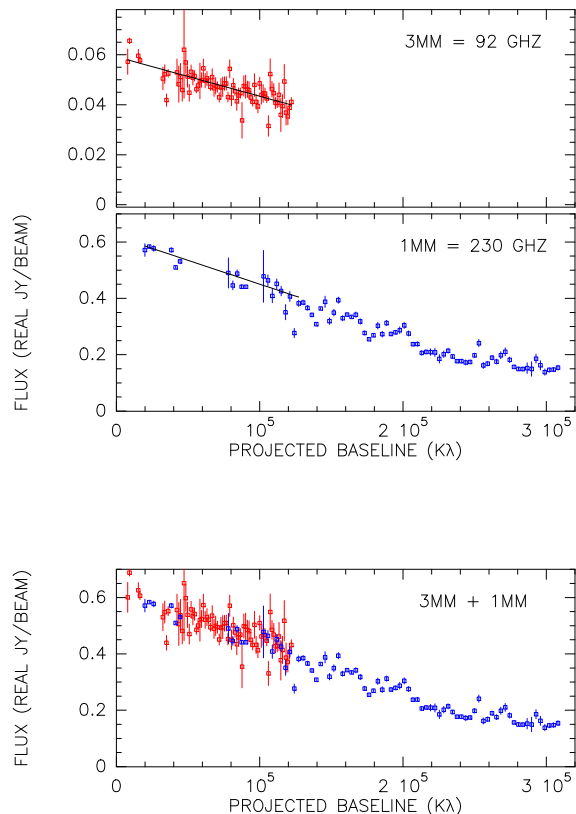


Fig. 2. Continuum visibilities at 92 GHz and 230 GHz vs projected baselines in units of wavelength. In the bottom panel we show together the 92 GHz and the 230 GHz visibilities. The 92 GHz visibilities have been scaled by a factor of 10.5 to match the 230 GHz ones. The perfect match between the 92 GHz and 230 GHz visibilities suggests that both emissions arise in the same region as expected in the case of dust thermal emission.

that the 3mm and 1.3mm emission arises in the same region and the spectral index larger than 2 is consistent with dust thermal emission. We have used the high-angular resolution 1.3mm image to model the continuum emission. Several models (elliptical Gaussian, disk, $F_\nu=\nu^{-2}$, $F_\nu=\nu^{-3}$, and an elliptical Gaussian+point source) have been used to fit the visibilities. The best fit has been obtained with the elliptical Gaussian+point source model. The HPFW of the elliptical Gaussian is $\sim 650 \times 900$ AU and the flux is 0.43 Jy. The point source has a flux of 0.13 Jy. The total flux of the compact 1.3 mm component is ~ 0.56 Jy. This implies a total (dust +gas) mass of $2 M_\odot$ assuming a standard dust temperature of 100 K and a dust emissivity $k_\nu=0.015(1300/\lambda (\mu\text{m})) \text{ cm}^2 \text{ g}^{-1}$. Taking into account the uncertainty in the value of the dust temperature which could range between 50 K and 300 K this mass is accurate within a factor of 4.

Table 1. Observations with the Plateau de Bure Interferometer (PdBI)

	Conf.	Beam	date
Continuum 3mm	A	1.56'' \times 1.20''	March 03
Continuum 1mm	A	0.63'' \times 0.46''	March 03
CH ₃ CN 5 _k →4 _k	A	1.56'' \times 1.20''	March 03
N ₂ D ⁺ 3→2	A	0.63'' \times 0.46''	March 03
D ₂ CO 4 ₀₄ →3 ₀₃	A	0.63'' \times 0.46''	March 03
CH ₃ OH 5 _{k,k'} →4 _{k,k'}	CD	1.51'' \times 1.42''	Nov, Dec 98

We speculate about the possibility that the point source is an accretion disk. In this case, the mass of the disk would be $\sim 0.3\text{--}0.8 M_{\odot}$. This value is 30 times larger than that found by Fuente et al. (2003) in the Herbig Be star R Mon, but it is similar to that found by Rodriguez et al. (2005) in the Class 0 low-mass protostar IRAS 16293–2422B. Thus, if our assumption is confirmed, the difference in the disk occurrence and masses between IM and low mass stars would be related to a short timescale for the disk dissipation instead of to differences in the first stages of the star formation. This interpretation is in line with Fuente et al. (2003).

4. Molecular line images

4.1. CH₃CN

The interferometric image of the Class 0 protostar NGC 7129–FIRS 2 in the CH₃CN 5→4 line shows a compact source at the same position and with the same size as the 1mm continuum source (Fig. 1). The total agreement in position and size between the continuum and the CH₃CN emissions points out to the existence of a well-differentiated compact component in the protostellar envelope.

Because of the rotational structure of CH₃CN, one can observe several lines at different energies very close in frequency. In Fig. 3 we show the interferometric spectrum of the CH₃CN 5→4 line compared to the single-dish spectrum reported in Paper II. The interferometer has recovered 100% of the flux of the highest upper state energy component ($E_u=124$ K) (see Fig. 3). However, only 37% of the flux of the lowest energy component ($E_u=13$ K) has been recovered (see Fig. 3). This suggests that while the emission of the low energy CH₃CN lines mainly arises in the cooler and more extended envelope, the emission of the high energy lines entirely arises in the hot core. In addition to the CH₃CN K-ladder we have also detected the CH₃¹³CN 5₀→4₀ line which allows us to have an estimate of the opacity of the CH₃CN line.

The CH₃CN column density has been estimated using the rotational diagram technique. The low energy lines are expected to be optically thick in the hot core. This is confirmed by our interferometric observations. In particular, we measure $I(\text{CH}_3\text{CN } 5_0\rightarrow 4_0)/I(\text{CH}_3^{13}\text{CN } 5_0\rightarrow 4_0)\sim 2.4$ which implies an opacity ~ 25 for the main isotope line

assuming $^{12}\text{C}/^{13}\text{C}=70$. We have corrected by the opacity effect and derived $T_{rot}\sim 54$ K and a beam averaged column density $N(\text{CH}_3\text{CN})\sim 1.1 \cdot 10^{16} \text{ cm}^{-2}$ for the hot core component using the 5₀→4₀ and 5₅→4₅ lines. The derived rotation temperature is in agreement, within the uncertainties, with that derived from single dish data (Fuente et al. 2005). Since the low energy lines are optically thick in the hot core, we think that this agreement is fortuitous and due to the addition of two uncertainties which shift the estimated column density in opposite directions, the contribution of extended emission in the single-dish beam and the opacity effect. From our interferometric observations, we obtain $X(\text{CH}_3\text{CN})\sim 7.0 \cdot 10^{-9}$ in the 2 M_{\odot} hot core in FIRS 2 assuming a source size of $0.72''\times 0.52''$ (see Table 5). This fractional abundance is similar to that measured in massive hot cores and slightly larger than those derived in hot corinos.

For comparison, we have estimated the CH₃CN abundance in the cooler and extended envelope. For this aim, we have subtracted the emission of the compact component from the single-dish spectrum and analyze the result using a rotational diagram. The opacity effect are expected to be less important in the low density envelope than in the hot core. We derive $T_{rot}=12$ K and a beam averaged column density of $5.8 \cdot 10^{11} \text{ cm}^{-2}$ (HPBW=25''). Using the H₂ column density derived from single-dish continuum observations by Fuente et al. (2001), we estimate a CH₃CN fractional abundance of $\sim 3 \cdot 10^{-11}$ in the extended component, i.e. about 3 orders of magnitude lower than in the compact component.

Summarizing, our CH₃CN interferometric data show the existence of a compact (900 \times 650 AU) source characterized by a high kinetic gas temperature (>50 K) and enhanced CH₃CN abundance ($X(\text{CH}_3\text{CN})\sim 7.0 \cdot 10^{-9}$) in the Class 0 IM protostar FIRS 2. This constitutes a definite proof of the existence of a hot core in this IM protostar which, up to our knowledge, it is the first IM hot core detected so far.

4.2. CH₃OH

We have observed the CH₃OH $J_{k,k'}=5_{k,k'}\rightarrow 4_{k,k'}$ lines towards FIRS 2 using the 2.5 MHz wide band correlator which allows us to observe most of the CH₃OH $J_{k,k'}=5_{k,k'}\rightarrow 4_{k,k'}$ components simultaneously. In Fig. 1 we show the total integrated intensity map of the CH₃OH 5_{1,4}→4_{1,4} line which is that observed with the lowest upper stage energy ($E_u=35$ K). The emission of this component presents two maxima, the first one is spatially coincident with the hot core while the second is located at the position ($-2''$, $-1.5''$). This position lies on the axis of the outflow FIRS 2-out 1. In Fig 1 we also show the integrated intensity map of the 5_{3,1}→4_{3,1}, 5_{3,2}→4_{3,2}, 5_{2,2}→4_{2,2} and 5_{3,3}→4_{3,3} lines [panel indicated as CH₃OH (high) in Fig. 1]. These lines are partially overlapped in our spectrum and all of them have upper state energies >50 K. In this case, the emission is mainly arising in the hot core

Table 2. Gaussian fits to the line and continuum emission

	Position ^a		Integrated intensity ^b (Jy)	Size ^c (arcseconds)
Continuum 3mm	21:43:01.7	66:03:23.6	0.0565(0.0005)	0.66(0.02)×0.54(0.02)
Continuum 1mm	21:43:01.7	66:03:23.7	0.4278(0.0047)	0.72(0.01)×0.52(0.01)
	21:43:01.7	66:03:23.6	0.1276(0.0046)	Point source (< 0.3 ^{''})
CH ₃ CN 5 _k →4 _k	21:43:01.7	66:03:23.6	0.0734(0.0060)	0.63(0.22)×0.46(0.19)
D ₂ CO 4 ₀₄ →3 _{0,3}	21:43:01.7	66:03:23.6	0.76(0.6)	0.58(0.24)×0.40(0.24)

^a The absolute positional precision is $\leq 0.3''$.

^b Systematic calibration errors are not included in the error budget associated to the integrated intensity

^c Deconvolved by the synthesized interferometric beam.

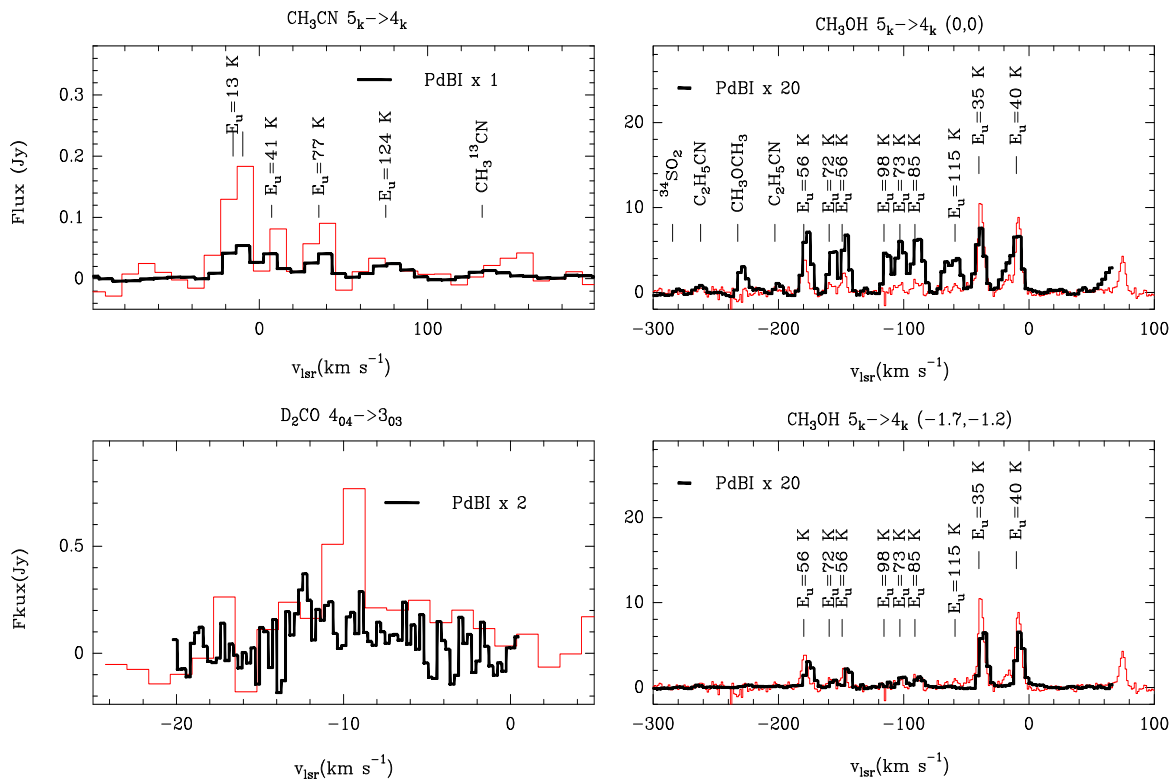


Fig. 3. Comparison between the single-dish (thin histograms or red) and interferometric (thick histograms or black) spectra towards the hot core position. The interferometric spectrum has been scaled for an easier comparison. Note that we have recovered all the flux for the CH₃CN line with the highest upper state energy.

with a very weak contribution of the second maximum. Thus, the morphology of the CH₃OH emission shows the existence of two components, a compact one which is spatially coincident with the hot core (hereafter hot core component) and an extended one which is very likely associated with the outflow FIRS 2–out 1 (hereafter outflow component).

In Fig. 3 we compare the interferometric spectra for the hot core and outflow components with the single-dish spectrum at the central position. The two components present differences in their kinematics and excitation conditions. The emission of the CH₃OH lines towards the hot core is centered at a velocity -10 ± 1 km s⁻¹, while the emission of the outflow component is centered at

-6 ± 1 km s $^{-1}$. The ^{12}CO 2 \rightarrow 1 and SiO 2 \rightarrow 1 maps of the outflow FIRS 2–out 1 reported in Paper II show that this velocity, -6 ± 1 km s $^{-1}$, is characteristic of the high velocity bullet R1, reinforcing our interpretation of this emission as associated with the bipolar outflow.

Different excitation conditions characterize the hot core and outflow components. This is clearly seen when one compares the relative intensities of the high and low energy lines in the methanol spectra towards the two studied positions. All the CH_3OH lines have similar intensities towards the hot core. However, high energy lines are a factor of ~ 5 weaker than the low energy ones towards the outflow position (see Fig. 3). We have derived the rotation temperature and the beam averaged CH_3OH column density for the hot core using the rotational diagram technique (see Fig. 4). We obtain $T_{\text{rot}}=809$ K and $N(\text{CH}_3\text{OH})=1.5 \cdot 10^{17}$ cm $^{-2}$. This temperature is quite high compared with that obtained from the CH_3CN lines. Similarly to the case of CH_3CN , the low energy lines are very likely optically thick and the derived rotation temperature is an upper limit to the actual one. To have an estimate of the uncertainty due to the unknown rotation temperature in the CH_3OH column density, we have calculated the CH_3OH column density from the flux of the $5_{4,3}\rightarrow 4_{4,3}$ line ($E_u=104$ K) assuming $T_{\text{rot}}=50$ K. We obtain $N(\text{CH}_3\text{OH})=4.9 \cdot 10^{16}$ cm $^{-2}$. Thus, we consider that our beam averaged column density estimate is accurate within a factor of 3. Assuming $T_{\text{rot}}=50$ K, the derived CH_3OH fractional abundance is $3.0 \cdot 10^{-8}$ in the hot core. This abundance is similar to that measured in the prototypical massive hot core OMC1.

For comparison, we have estimated the rotation temperature and methanol column density for the outflow condensation (see Fig. 4). We have obtained $T_{\text{rot}}=19$ K and $N(\text{CH}_3\text{OH})=2.9 \cdot 10^{15}$ cm $^{-2}$. The low rotational temperature of this component supports our interpretation of being associated with the outflow (postshocked material) instead of with the hot core. We have not detected a millimeter continuum counterpart for this condensation in our interferometric 1mm map. In principle, this could be a sensitivity problem. From our interferometric image and assuming $T_{\text{dust}}=100$ K we derive a $3\times\sigma$ upper limit of $\sim 0.01 M_\odot$ for the mass of the condensation associated with the methanol clump. This would imply $X(\text{CH}_3\text{OH})>3.8 \cdot 10^{-7}$ in this clump. We can alternatively think that this clump is not the result of a hydrogen density enhancement at this position. For example, it could be produced by a local enhancement of the CH_3OH abundance because of the shocks associated with the bipolar outflow. To estimate the methanol abundance in this case, we calculate the H_2 column density from the single-dish ^{13}CO observations reported in Paper II. At the velocities of the bullet R1, the ^{13}CO column density averaged in the 30m beam is $\sim 3 \cdot 10^{15}$ cm $^{-2}$. If we assume a uniform distribution of the molecular gas in the beam, we obtain that the CH_3OH abundance is similar to that of ^{13}CO for which we assume a standard value of $\sim 10^{-6}$. Obviously, this is an upper limit to the actual abundance since we

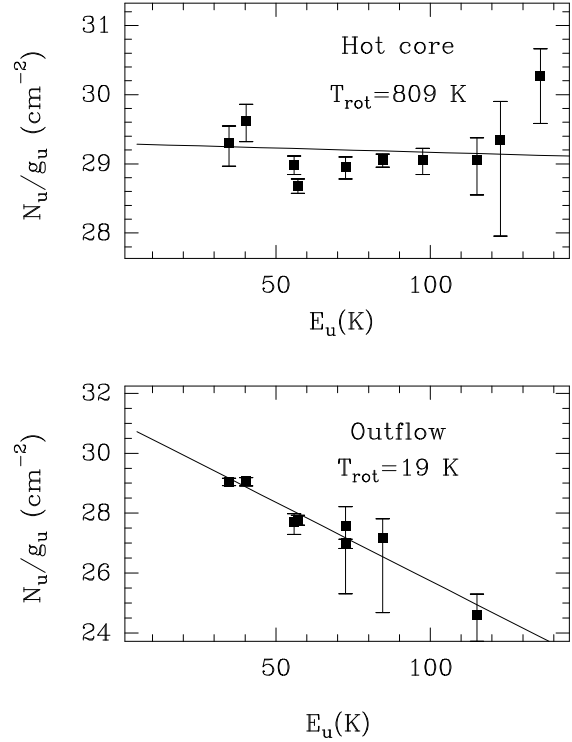


Fig. 4. Rotational diagram of CH_3OH towards the hot core and the outflow condensation. Note that the rotation temperature towards the hot core is much larger than towards the outflow condensation.

expect some clumpiness. Thus, the CH_3OH abundance in the outflow condensation could be larger than in the hot core and reach values close to 10^{-6} . This large value of the methanol abundance is consistent with those found in the molecular bullets associated with low-mass bipolar outflows (see e.g. Bachiller & Pérez-Gutiérrez 1997).

In addition to the CH_3OH lines, the spectrum towards the hot core show several lines that are weaker towards the outflow condensation. We have identified these lines as belonging to the complex molecules CH_3OCH_3 and $\text{C}_2\text{H}_5\text{CN}$. We have also a tentative detection of the sulphuretted species $^{34}\text{SO}_2$. The detection of complex saturated molecules corroborates the existence of a hot core in this source and reveals the rich and complex chemistry associated with it.

4.3. D_2CO

The interferometric map of D_2CO shows a compact source located at the position of the hot core (see Fig. 1). The size of the D_2CO emitting region is similar to that of CH_3CN . However, the linewidth of the D_2CO line is ~ 11 km s $^{-1}$, larger than those of the CH_3CN and CH_3OH lines which are typically ~ 6 – 8 km s $^{-1}$. Assuming the standard inside-outside collapse model, the largest linewidth of the D_2CO line is consistent with the emission arising in an inner

region of the protostellar envelope. In a simple calculation, an accretion velocity of ~ 5 km s $^{-1}$ corresponds to a radius of ~ 130 AU assuming a dynamical age of $\sim 10^5$ yr and $dM/dt = 5 \cdot 10^{-5} M_{\odot}$ yr $^{-1}$. A similar radius was found by Maret et al. (2004) for the region where the H₂CO abundance is heavily enhanced because of evaporation of the grain mantles in low-mass protostars. This suggests a similar origin for the D₂CO molecules in the hot core.

Our previous single dish spectrum was too noisy to detect this wide emission (Paper II). Recently, we have taken a good signal-to-noise ratio spectrum to compare with the interferometric observations (see Fig. 3). The single-dish spectrum shows two components, a narrow one at the velocity of the ambient cloud (already detected in Paper II) which is completely missed in our interferometric observations and a wide one with a linewidth similar to that of the PdB spectrum. Even in this wide component the interferometer recovers only the 50% of the flux, suggesting that part of them arises in a more extended area.

A narrow and wide components with linewidths similar to those of D₂CO are also detected in the single dish spectra of the H₂CO lines (Paper II). In Paper II, we have separately mapped the narrow and wide components. These maps revealed that both components are associated with the outflow. While the wide component arises in the jet, the emission of the narrow component was more intense in the interface between the jet and the molecular cloud suggesting that it is tracing the molecular gas that is being swept up by the jet. We propose that the missed flux in our interferometric D₂CO image is probably arising in a more extended component associated with the bipolar outflow similarly to the case of H₂CO.

Our interferometric image shows that, in addition to the extended component, there is an intense and compact D₂CO component associated with the hot core. We have estimated the D₂CO abundance in this component assuming $T_{rot} = 50$ K and obtained $N(D_2CO) = 3.5 \cdot 10^{14}$ cm $^{-2}$ and $X(D_2CO) \sim 1.4 \cdot 10^{-10}$. This fractional abundance is a factor of ~ 2 higher than that derived in Paper II for the whole envelope.

4.4. N₂D⁺

We have not detected the N₂D⁺ 3 \rightarrow 2 line in our interferometric image. The rms of the image is 50 mJy/beam which is about $\sim 2\%$ of the flux measured with the 30m telescope (Paper II). Thus, almost the 100% of the N₂D⁺ emission has been missed in the interferometric observations. This implies that the emission of N₂D⁺ presents a quite uniform distribution across the envelope and suggests that it mainly arises in the cooler extended envelope. This is also in agreement with our interpretation in Paper II based on kinematical arguments. The linewidth of the N₂D⁺ 3 \rightarrow 2 line, ~ 1 km s $^{-1}$, is at least a factor of 2–3 smaller than those of the lines arising in the warm component, and similar to those of the molecules which are

Table 3. USB - 2.4 MHz

Freq.	Molecule	Transition	Int ^a	E _u (K)
231060.98	OCS	19 \rightarrow 18	-2.6263	100
231187.69	CH ₃ OCHO-E	21 _{9,13} \rightarrow 21 _{8,14}	-4.8522	179
231199.96	CH ₃ OCHO-A	21 _{9,12} \rightarrow 21 _{8,13}	-4.8484	179
231200.14	CH ₃ OCHO-E	21 _{9,12} \rightarrow 21 _{8,13}	-4.8522	179
231220.99	¹³CS	5 \rightarrow 4	-4.2103	51
231229.96	NO ₂	4 _{1,3} \rightarrow 4 _{0,4}	-4.8527	12
231239.07	CH ₃ OCHO-A	21 _{9,13} \rightarrow 21 _{8,14}	-4.8482	179
231232.06	CH ₃ OCHO-E	29 _{6,24} \rightarrow 29 _{5,25}	-5.0160	253
231248.31	CH ₃ OCHO-E	29 _{6,24} \rightarrow 29 _{4,26}	-5.3013	253
231252.98	NO ₂	4 _{1,3} \rightarrow 4 _{0,4}	-5.0896	12
231279.18	CH ₃ CHO-A	12 _{6,7} \rightarrow 11 _{6,6}	-2.9783	142
231279.18	CH ₃ CHO-A	12 _{6,6} \rightarrow 11 _{6,5}	-2.9783	142
231286.40	CH ₃ OH	10 _{2,2} \rightarrow 9 _{3,2}	-4.0689	154
231287.14	NO ₂	4 _{1,3} \rightarrow 4 _{0,4}	-5.0875	12
231310.42	C₂H₅CN	26 _{1,25} \rightarrow 25 _{1,24}	-2.6517	142
231320.82	CH ₃ CHO-A	12 _{5,8} \rightarrow 11 _{5,7}	-2.9001	117
231320.97	CH ₃ CHO-A	12 _{5,7} \rightarrow 11 _{5,6}	-2.9001	117
231365.80	c-C₃D	5 _{3,3} \rightarrow 4 _{3,2}	-3.1276	28
231410.27	D₂CO	4 _{0,4} \rightarrow 4 _{0,3}	-2.4242	17
231446.49	CH ₃ CHO-A	12 _{4,9} \rightarrow 11 _{4,8}	-2.8386	97
231457.25	CH ₃ CHO-A	12 _{4,8} \rightarrow 11 _{4,7}	-2.8386	97
231485.11	c-C₃D	5 _{3,3} \rightarrow 4 _{3,2}	-3.4082	28
231505.70	HCOOH	10 _{1,9} \rightarrow 9 _{1,8}	-3.1963	53
231511.81	CH ₃ OCHO-E	27 _{4,24} \rightarrow 27 _{2,25}	-5.3849	211
231513.06	CH ₃ OCHO-E	27 _{4,24} \rightarrow 27 _{3,25}	-5.1294	211
231558.55	C₂H₅OH	21 _{5,17} \rightarrow 21 _{4,18}	-3.6252	215
231559.62	CH ₃ OCHO-E	27 _{5,23} \rightarrow 27 _{2,25}	-5.1292	211
231560.90	C₂H₅OH	20 _{5,16} \rightarrow 20 _{4,17}	-3.6250	197

^a Base 10 logarithm of the integrated intensity in units of nm²-MHz as appears tabulated in the JPL molecular line catalogue (Pickett et al. 1998).

Table 4. LSB - 2.4 MHz

Freq.	Molecule	Transition	Int ^a	E _u (K)
228122.07	CH ₃ OCHO-A	5 _{4,2} \rightarrow 4 _{2,3}	-7.1993	8
228134.42	c-C₃HD	15 _{7,8} \rightarrow 15 _{7,9}	-3.9965	288
228147.97	CH ₃ OCHO-E	18 _{6,13} \rightarrow 18 _{2,16}	-5.9576	114
228165.01	CH ₃ OCHO-A	18 _{6,13} \rightarrow 18 _{4,14}	-5.9537	114
228165.86	CH ₃ OCHO-E	44 _{14,31} \rightarrow 43 _{11,32}	-5.9853	673
228270.42	CH ₃ OCHO-A	24 _{9,16} \rightarrow 24 _{8,17}	-4.8334	220
228272.26	S ¹⁸ O	9 ₈ \rightarrow 8 ₈	-3.9573	82
228288.69	C₂H₅OH	11 _{11,0} \rightarrow 10 _{2,8}	-4.0647	107
228205.84	CH ₃ OCHO-E	24 _{9,16} \rightarrow 24 _{8,17}	-4.9577	220
228232	Unidentified			
228245	Unidentified			
228278.96	HCCCHO	25 _{1,25} \rightarrow 24 _{1,24}	-2.8001	135
228310.56	C ₂ H ₃ CHO	13 _{2,12} \rightarrow 12 _{1,11}	-4.6934	36
228358.20	CH ₃ OCHO-E	24 _{9,15} \rightarrow 24 _{8,17}	-5.4380	220
228415.69	c-C₃HD	11 _{8,4} \rightarrow 11 _{6,5}	-4.5197	169
228434	Unidentified			
228467	Unidentified			
228483.13	C₂H₅CN	25 _{2,23} \rightarrow 24 _{2,22}	-5.4674	158
228494.88	CH ₃ OCHO-E	14 _{4,10} \rightarrow 14 _{1,13}	-6.2908	3
228522.71	C₂H₅OH	7 _{3,4} \rightarrow 7 _{2,6}	-4.3308	84
228544.17	HCOOH	10 _{2,8} \rightarrow 9 _{2,7}	-3.2324	62

^a The same as in Table 3.

thought to be good tracers of the cold envelope such as H¹³CO⁺ and N₂H⁺.

5. Chemical complexity of the hot core in NGC 7129–FIRS 2

In Fig. 5 we show the observed wide band spectra in the upper side band (USB) and lower side band (LSB) of the 1mm receiver. We have detected a real forest of lines in the 1mm band. The identification of these lines is not an easy task. Since we have moderate spectral resolution (2.5

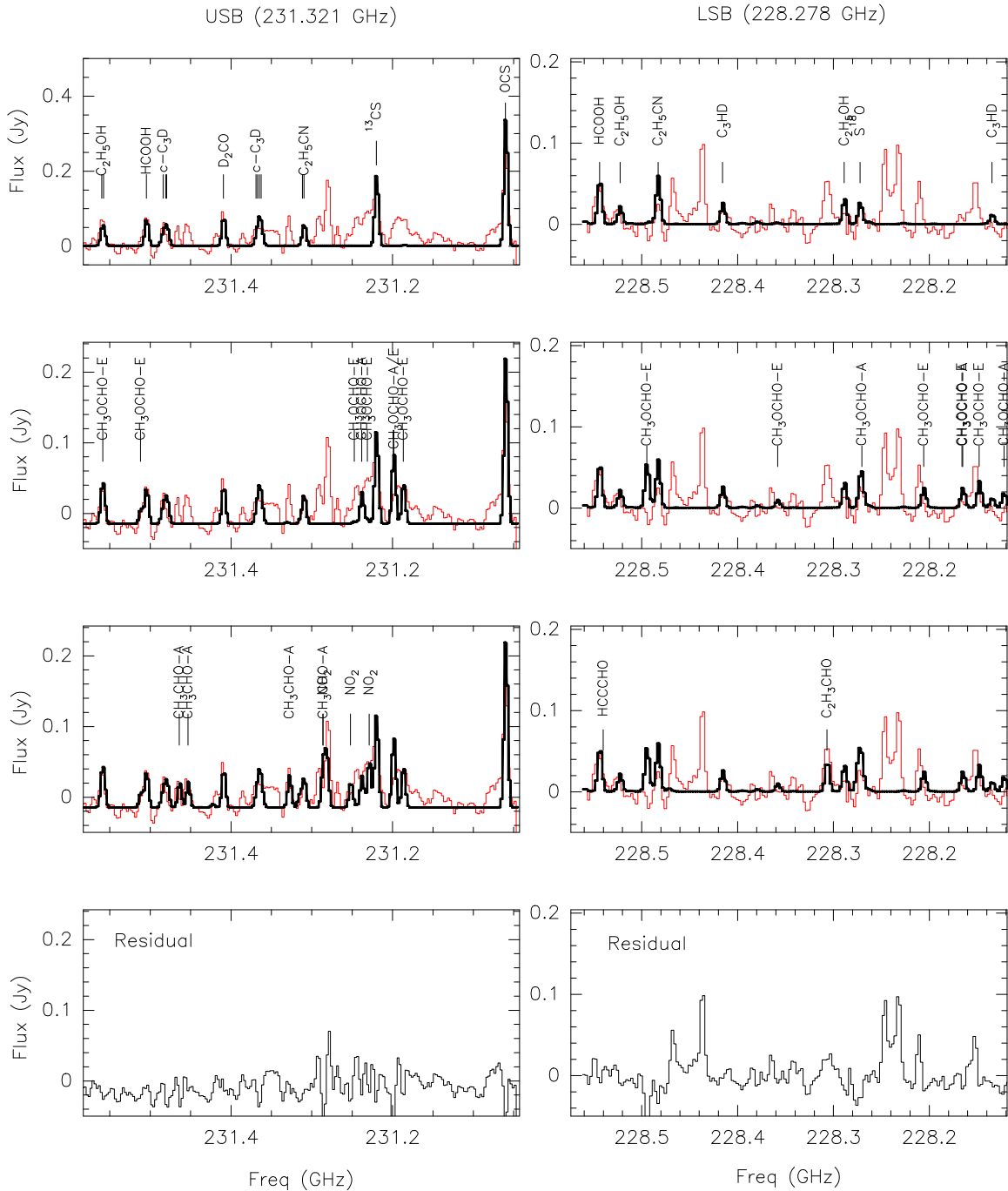


Fig. 5. Spectra of the upper side band (USB) and lower side band (LSB) of the 1mm receiver obtained in our PdBI observations with our best guess for line identifications. For clarity, we have divided the molecular species in three groups. The first group is formed by the more reliable identifications and $S^{18}O$. Beginning from the top, in the first line of panels we compare the observed spectra with the synthesized ones taking into account only this first group. In the second line, we add $CH_3OCHO-A/E$ and show the obtained synthesized spectra. The inclusion of these compounds improve the agreement with the observational data. However, the large $CH_3OCHO-A/E$ abundance we derive from these observations, rise some questions about this identification. In the third line of panels, we show the synthesized spectra after adding some other exotic compounds. In the last line, it is shown the residual spectra after subtracting our fit. Note that the agreement between the synthesized and observed one is very good in the USB but some lines remain unidentified in the LSB.

Table 5. Fractional Abundances in the hot core of NGC 7129–FIRS 2 and comparison with other hot cores

Molecule	T_{rot} (K)	NGC 7129–FIRS 2		NGC 1333 IRAS4 A	IRAS 16293	OMC 1	G327.3-0.6
		$\sim 500 L_{\odot}$	X^a	$\sim 14 L_{\odot}$	$\sim 23 L_{\odot}$	$\sim 1.0 L_{\odot}^4$	$\sim 10^5 L_{\odot}$
		$N^* (\text{cm}^{-2})$		X^b	X^c	X^d	X^e
H₂		7.9×10^{24}	1	1	1	1	1
CH₃CN	54	5.5×10^{16}	7.0×10^{-9}	1.6×10^{-9}	1.0×10^{-8}	4×10^{-9}	7×10^{-7}
CH₃OH	50 ^a	2.4×10^{17}	3.0×10^{-8}	$< 7 \times 10^{-9}$	3.0×10^{-7e}	1×10^{-7}	2×10^{-5}
H₂CO	50 ^a	2.5×10^{15}	3.1×10^{-10}	2.0×10^{-8}	6.0×10^{-8}	7.0×10^{-9}	
D₂CO	50 ^a	3.5×10^{14}	4.4×10^{-11}		3.0×10^{-9g}		
¹³CS	50 ^a	3.4×10^{14}	4.3×10^{-11}			7×10^{-11}	5×10^{-11g}
OCS	50 ^a	2.4×10^{16}	3.0×10^{-9}		1.0×10^{-6}	7×10^{-8}	2×10^{-8g}
HCOOH	48	3.5×10^{15}	4.4×10^{-10}	4.6×10^{-9}	6.2×10^{-8}	8×10^{-10}	3×10^{-10h}
C₂H₅OH	75	2.0×10^{16}	2.5×10^{-9}			7×10^{-10}	3×10^{-9h}
C₂H₅CN	50 ^a	3.2×10^{15}	4.0×10^{-10}	$< 1.2 \times 10^{-9}$	1.2×10^{-8}	3.0×10^{-9}	4×10^{-7}
c-C₃D	50 ^a	2.5×10^{15}	3.1×10^{-10}				
c-C₃HD	50	1.8×10^{17}	2.3×10^{-8}				
Uncertain identifications							
S¹⁸O	50 ^a	2.6×10^{16}	3.3×10^{-9}		2.6×10^{-9}	3×10^{-10}	$> 6 \times 10^{-13}$
CH₃OCHO-E	36	4.0×10^{18}	5.0×10^{-7}	3.6×10^{-8}	2.3×10^{-7}	1×10^{-8}	2×10^{-6}
CH₃OCHO-A	36 ^a	3.3×10^{18}	4.1×10^{-7}	3.4×10^{-8}	1.7×10^{-7}	1×10^{-8}	2×10^{-6}
CH₃CHO-A	50 ^a	2.3×10^{15}	2.9×10^{-10}		1.9×10^{-8}		5×10^{-10g}
HCCCHO	50 ^a	2.0×10^{15}	2.5×10^{-10}				
C₂H₃CHO	50 ^a	5.0×10^{16}	6.3×10^{-9}				
CH₃OCH₃	50 ^a	1.9×10^{15}	2.4×10^{-10}	$< 2.8 \times 10^{-8}$	2.4×10^{-7}	8×10^{-9}	3×10^{-8g}
³⁴SO₂	50 ^a	3.8×10^{13}	4.8×10^{-12}		2.4×10^{-8}	2×10^{-10}	4×10^{-9g}
NO₂	50 ^a	1.0×10^{17}	1.2×10^{-8}				

* Values derived for the NGC 7129–FIRS 2 hot core assuming a size of $\sim 0.72'' \times 0.52''$. To derive the H₂ column density we have considered that the hot core mass (2 M_⊙) is uniformly distributed in an area $\sim ab$ with $a=0.004$ pc (0.72'') and $b=0.003$ pc (0.52'').

^a Assumed temperature.

^b Values from Bottinelli et al. (2004) for a 0.0016 pc (0.5'') source.

^c Values from Cazaux et al. (2003) and Wakelam et al. (2004) for a 0.0016 pc (2'') source.

^d Values from Sutton et al. (1995) for a 0.034 pc (14'') source.

^e Values from Gibb et al. (2000) for a 0.03 pc (2'') source.

^f From Schoier et al. (2002).

^g From Ceccarelli et al. (2001).

^h From Gibb et al. (2000) for a 0.32 pc (20'') source.

MHz), several candidates can be found for each line. On the other hand, in most cases we have two or more lines overlapped. We have tried to identify most of them with the following procedure: In a first step we select our best candidates for the lines and estimate the column density of the carriers assuming optically thin emission and local thermodynamic equilibrium (LTE). In a few cases, we are able to estimate the rotation temperature because we have at least two ‘‘isolated’’ lines (see Table 3). In the other cases, we have assumed $T_{rot}=50$ K. In a second step, we synthesized the expected spectrum assuming the estimated column densities. The velocity profile is assumed to be Gaussian with a half power full width of 7 km s⁻¹ and centered at the ambient cloud velocity, -10 km s⁻¹. Finally, we compare it with the observed spectrum and readjust the molecular column densities to improve the fit. We list in Tables 3 and 4 the lines detected in the USB and LSB spectra with the most likely line identification.

Obviously, this identification procedure entails some ambiguity. We have classified the species according with the reliability of their identification in two groups that are differentiated in Table 5. The first group contains the most reliable identifications. In these cases, the observed frequencies are in total agreement with those calculated for these species. Moreover, the synthesized spectrum matches quite well with the observed one (see top panel of Fig. 5). Finally, the derived fractional abundances are within the range of abundances measured for these species in hot cores. Within this group, we have OCS, ¹³CS, C₂H₅CN, c-C₃D, D₂CO, HCOOH, and C₂H₅OH in the USB and C₂H₅OH, C₃HD in the LSB. The lines of the first group species are indicated by bold characters in Tables 3 and 4. The derived column densities and fractional abundances are shown in Table 5.

We have put the complex molecules CH₃OCHO-A and CH₃OCHO-E (methyl formate) in the second group. Several lines of these species have been detected in the

USB and LSB (see second panels in Fig. 5). However, the derived fractional abundances in NGC 7129-FIRS 2 are unexpectedly high compared to those measured in hot corinos and massive hot cores (see Table 3). One possibility is that the rotation temperature is higher than that assumed. To estimate the uncertainty due to the poorly known rotation temperature, we have repeated the column density calculations with $T_{rot}=300$ K. The derived abundance is an order of magnitude lower and then it agrees with that derived in IRAS 16293. This high rotation temperature could be explained if this complex molecule arises in an inner and hotter region than CH_3CN . If methyl formate cannot be produced in the gas phase (as suggested by the laboratory results of Horn et al. 2004), our findings may imply that this species is formed on grain surfaces and that its binding energy is larger than that of CH_3CN , thus requiring larger dust temperatures to desorb.

The rarer isotope S^{18}O has also been included in the group of uncertain identifications. We have only one line of this molecule, $\text{S}^{18}\text{O } 9_8 \rightarrow 8_8$ at 228.272 GHz, and the derived S^{18}O abundance is unexpectedly high. In this case we could have a misidentification. There is a CH_3OCHO -A line at 228.270 GHz, that could be an alternative identification of the tentative S^{18}O line if the methyl formate abundance is unexpectedly high.

The most uncertain identifications are $\text{C}_2\text{H}_3\text{CHO}$, CH_3CHO -A, HCCCHO , and NO_2 . The observed frequencies are in agreement with those of $\text{C}_2\text{H}_3\text{CHO}$, CH_3CHO -A, and HCCCHO lines if the emission arises in gas at a velocity $v_{lsr} \approx -5$ km s $^{-1}$. This velocity is coincident with that of the bullet R1 (see Paper I) but is shifted by ~ 5 km s $^{-1}$ from that of the molecular cloud. Similarly, the fit to the USB spectrum improves if we include a high excitation methanol line (see Table 3) emitting at the velocities -5 and -20 km s $^{-1}$. These velocities are within the range of velocities associated with this Class 0 protostar but are shifted from that of the ambient cloud. NO_2 is not a common molecule in hot cores, and the three lines observed in the spectrum are overlapped with others of more common hot core species. We have kept it in the table because its inclusion improves the fit to the observed spectrum.

In Fig. 5 we show the synthesized USB and LSB spectra assuming the molecular column densities listed in Table 3. The fit is quite good for the USB. However, it is poor for the LSB where we still have 4 unidentified lines. This is quite frustrating taking into account that they are the most intense lines in this subband. The frequencies of the unidentified lines are 228467(± 5), 228434(± 5), 228245(± 5) and 228232(± 5) MHz, and we do not have any good candidates for them. There is a line of vibrationally excited DC_3N at the frequency of 228467.44 GHz. Emission of vibrationally excited HC_3N has been detected in massive hot cores (see e.g. Wyrowski et al. 1999). However, if this identification were correct, we would expect to see a vibrationally excited HC_3N line at least ten times more intense at a frequency of 228303 MHz which is not detected. For the line at 228434 MHz our best can-

didate is glycoaldehyde ($\text{CH}_2(\text{OH})\text{CHO}$). Glycoaldehyde has already been observed in the interstellar medium (Hollis et al. 2004). However, the upper state energy of the line at 228434 MHz is too high (>1400 K) to be detectable in this source. The line at 228245 MHz could be propadienone (CH_2CCO), but in this case we should have detected other lines of this compound in the same spectrum. Finally, our best candidate for the line at 228232 MHz is cyclopropanone ($\text{C}_3\text{H}_2\text{O}$). This molecule has never been detected in space. Since we have only one observable line in our spectra, we cannot confirm this detection.

In addition to the lines detected in the wide-band spectrum shown in Fig. 5, in Table 5 we also include the column densities derived for CH_3OCH_3 and $^{34}\text{SO}_2$, these species detected in the CH_3OH spectrum shown in Fig. 3. Since we have only one line for these species, the derived column density is also uncertain.

6. Discussion

In Table 5 we list the derived abundances of the molecules detected in the hot core towards FIRS 2. A first look at the Table reveals that FIRS 2 is rich in deuterated species (D_2CO , $c\text{-C}_3\text{D}$ and $c\text{-C}_3\text{HD}$), sulphuretted compounds (^{13}CS , OCS) and complex O- and N- molecules (HCOOH , $\text{C}_2\text{H}_5\text{OH}$, $\text{C}_2\text{H}_5\text{CN}$). Taking into account the large uncertainty in the estimated fractional abundances, we have centered our discussion in the most reliable identifications, i.e., the first group in Table 3.

6.1. Deuterated species

The deuterium fractionation of molecular species is a well known process in dense interstellar clouds (Watson, W.D. 1974). In the gas phase, this is mainly driven by the enhancement of the $\text{H}_2\text{D}^+/\text{H}_3^+$ ratio due to the exothermic proton-deuteron exchange reaction $\text{H}_3^+ + \text{HD} \rightarrow \text{H}_2\text{D}^+ + \text{H}_2$ ($+ 230$ K), which does not proceed backwards if the gas temperature is less than about 30 K. This process is responsible for the deuteration of species such as HCO^+ and N_2H^+ , via the reaction of H_2D^+ with the parent species CO and N_2 , respectively, as observed in dense cloud cores (Butner et al. 1995; Williams et al. 1998).

Another phenomenon which boosts the deuterium fractionation is the freeze out of neutral species, in particular the abundant O and CO, which are efficient destruction partners of H_3^+ and H_2D^+ in the gas phase. Their freeze out, known to happen in dense cold clouds (Williams et al. 1998; Caselli et al. 1999; Kramer et al. 1999; Bergin et al. 2002; Tafalla et al. 2002), further enhances the $\text{H}_2\text{D}^+/\text{H}_3^+$ abundance ratio (because of the enhanced formation rate of H_2D^+ , and the reduced destruction rates for H_2D^+ and H_3^+) and the consequent transfer of the deuteron to gas-phase species (Caselli et al. 2002; Bacmann et al. 2003; Crapsi et al. 2005). Once CO is highly depleted, multiple deuterated forms of H_3^+ can easily be produced (Roberts et al. 2003; Walmsley et al. 2004). Indeed, large

abundances of H_2D^+ and D_2H^+ have been measured toward two pre-stellar cores (Caselli et al. 2003; Vastel et al. 2004). This has the consequence of enhancing the gaseous D/H ratio to values around 0.1, four orders of magnitude larger than the cosmic D abundance, which allows an efficient deuteration on grain surfaces (Tielens 1983; Charnley et al. 1997; Stantcheva & Herbst 2003).

We have detected the deuterated species D_2CO , $c\text{-C}_3\text{D}$ and $c\text{-C}_3\text{HD}$ towards FIRS 2. Moreover, the D_2CO interferometric image shows that the D_2CO emission is strongly peaked towards the hot core position. Recent theoretical and observational research suggests that the abundance of the non-deuterated species H_2CO is enhanced by more than 2 orders of magnitude in the inner region of the envelope, where the dust temperature is larger than 100 K (Maret et al. 2004). The size of this region (~ 100 AU) is similar to that derived for the D_2CO emission from the linewidth of the D_2CO line. Assuming that evaporation is also the origin of D_2CO , the $[\text{D}_2\text{CO}]/[\text{H}_2\text{CO}]$ would tell us about the gaseous D/H ratio during the pre-stellar phase of the parent clump. Unfortunately, we have not interferometric observations of H_2CO and cannot derive an accurate $[\text{D}_2\text{CO}]/[\text{H}_2\text{CO}]$ ratio in the hot core. Trying to get an estimate of the deuteration degree of formaldehyde, we have compared the single dish spectra of the D_2CO $4_{04}\rightarrow 3_{03}$ and H_2CO $3_{12}\rightarrow 2_{11}$ lines (see Fig. 6). Both lines have similar excitation conditions and frequency. The line intensity ratio in the narrow component is lower by a factor of 2 than in the wide component suggesting a higher $[\text{D}_2\text{CO}]/[\text{H}_2\text{CO}]$ ratio in the hot core. Assuming the same physical conditions for D_2CO and H_2CO we derive $[\text{D}_2\text{CO}]/[\text{H}_2\text{CO}]\sim 0.14\pm 0.03$ in the hot core. This value is similar to that found in pre-stellar cores and low-mass protostars (Caselli et al. 2002; Bacmann et al. 2003; Ceccarelli et al. 2001; Loinard et al. 2003) and it implies large D/H ratios during the cold pre-stellar phase ($\text{D}/\text{H}\sim 0.5$, see Caselli et al. 2002b; Stantcheva & Herbst 2003).

Contrary to D_2CO , we have not detected N_2D^+ in our interferometric observations. It is interesting to note that whereas the deuteration of N_2H^+ is a gas-phase process (which proceeds from the reaction between N_2 and H_2D^+), the formation of D_2CO seems to require surface chemistry (Ceccarelli et al. 2002). Therefore, our result is not surprising. In fact, as stated above, the deuteration in the gas phase is efficient only if the gas temperature is lower than, say, 30 K. Thus, in a hot core, we do not expect to see N_2D^+ . Moreover, in hot cores, where icy grain mantles evaporates, CO and H_2O molecules are abundant in the gas phase and they efficiently destroy N_2H^+ (and N_2D^+), so that one does not expect to see large abundances of N_2H^+ either. The non-detection of N_2D^+ in the hot core associated with FIRS 2 confirms the interpretation given in Paper II that N_2D^+ mainly arises in the cool envelope, and constitutes an indirect proof of this chemical scheme. On the other hand, the large $\text{D}_2\text{CO}/\text{H}_2\text{CO}$ abundance ratio observed in the same position can be easily explained

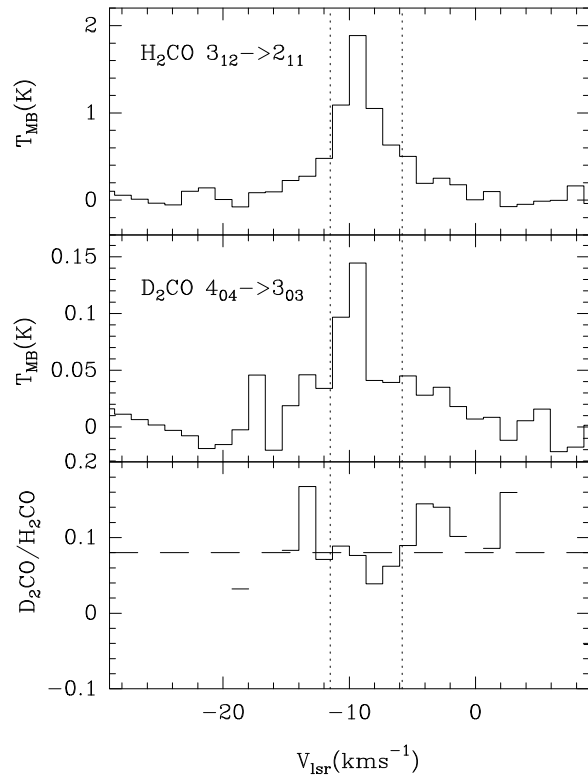


Fig. 6. Single-dish spectra of the H_2CO $3_{12}\rightarrow 2_{11}$ and D_2CO $4_{04}\rightarrow 3_{03}$ lines towards FIRS 2. In the bottom panel we show the $I(\text{D}_2\text{CO } 4_{04}\rightarrow 3_{03})/I(\text{H}_2\text{CO } 3_{12}\rightarrow 2_{11})$ line ratio. Note that this ratio presents a minimum around the velocity of the ambient cloud (~ -10 km s^{-1}).

if the deuterium fractionation of formaldehyde happened on grain surfaces during the cold pre-stellar phase, and if icy mantles have recently evaporated, so that gas phase chemistry did not have the time to significantly reduce the abundance of the deuterated “parent” species.

6.2. Sulphuretted species

The abundances of sulphuretted molecules are very dependent on the stellar age. We have compared the observed $[\text{CS}]/[\text{OCS}]$ ratio in FIRS 2 (~ 1.1 assuming $\text{CS}/^{13}\text{CS}=89$) with the Viti et al. (2004) model for a $5 M_{\odot}$ star. The measured ratio is consistent with the FIRS 2 being an evolved hot core with an age of $>1.0 \cdot 10^5$ yr. The detection of large species like $\text{C}_2\text{H}_5\text{OH}$ also suggests that we are dealing with an evolved hot core since these species are only formed at late times. Nevertheless, we would like to point out that the determination of the hot core age using the sulphuretted molecules is quite uncertain since other factors like the ice mantle composition and the hot core kinetic temperature can also strongly affect the abundances of these species (Wakelam et al. 2004).

6.3. Complex O- and N-bearing molecules

Theoretical models predict that the relative abundance of the N-bearing and O-bearing complex molecules is dependent on the hot core temperature (Caselli et al. 1993; Rodgers & Charnley 2001). The luminosity of FIRS 2 is a factor >10 larger than those of the two low mass hot corinos detected so far and a factor ~ 200 lower than that of the massive protostar creating the Orion hot core. The intermediate kinetic temperature of the FIRS 2 hot core is expected to produce a differentiated chemistry of complex molecules. In order to have a deeper insight into the dependence of the complex molecules abundances on the protostellar luminosity, in Table 5 we compare the observed abundances towards FIRS 2 with those measured in prototypical hot corinos and massive hot cores. The luminosity of the objects listed in Table 5 varies by 4 orders of magnitude, thus one expects to detect some chemical differences between these hot cores.

However, the comparison of abundances between different hot cores (corinos) is difficult. First of all, since massive stars are usually located farther from the Sun than their low- and intermediate-mass counterparts, the abundances are derived in different spatial scales. The fractional abundances shown in Table 5 are averaged values in regions with sizes ranging from ~ 0.002 pc in NGC1333–IRAS 4A to 0.32 pc in OMC1 and G327. These sizes are given by the angular resolution of the current instrumentation at the hot core distance. Thus, the derived abundances in massive hot cores would be severely underestimated in the case of sizes similar to those of hot corinos. On the other hand, we can have several hot cores in the studied region, specially in massive star forming regions where clustering is more important and are located at greater distances. In order to minimize these problems, we normalize the studied abundances to those of the parent species.

As a first step, we have normalized all the molecular abundances to that of H_2CO and CH_3OH . These species are thought to be the “parent” molecules of complex O-bearing species, although some doubts are cast in the particular case of methyl formate (Horn et al. 2004). In Fig. 7a, we show the relative abundances of HCOOH , CH_3OH , CH_3CN and $\text{C}_2\text{H}_5\text{CN}$ respect to H_2CO as a function of the luminosity. Since we have not interferometric observations of H_2CO in FIRS 2, we have estimated the H_2CO abundance assuming $[\text{D}_2\text{CO}]/[\text{H}_2\text{CO}]=0.014$. A clear trend is observed in the relative abundance of CH_3OH , CH_3CN and $\text{C}_2\text{H}_5\text{CN}$ respect to H_2CO as a function of the stellar luminosity (Fig. 7a). The abundance of all these molecules increases by a factor of ~ 10 from NGC 1333–IRAS 4A ($L=14 L_\odot$) to OMC1 ($L=10^4 L_\odot$). This trend does not present significant differences between O- and N-bearing molecules. Contrary to these molecules, the $[\text{HCOOH}]/[\text{H}_2\text{CO}]$ ratio does not present a systematic behavior.

In Fig. 7b we plot the abundances of the same molecules normalized to that of CH_3OH . Different be-

haviors are found for the different molecules. The $[\text{CH}_3\text{CN}]/[\text{CH}_3\text{OH}]$ ratio does not present any systematic trend with the protostellar luminosity, although the dispersion in the values is quite high. The same remains true for $\text{C}_2\text{H}_5\text{CN}$ and probably for $\text{C}_2\text{H}_5\text{OH}$ (we only have 3 points for $\text{C}_2\text{H}_5\text{OH}$). This suggests that the ratio between O- and N-bearing complex molecules does not seem to strongly depend on the protostellar luminosity, contrary to that expected from theoretical models. However, the relative abundance of HCOOH seems to decrease by 2 orders of magnitude from NGC 1333–IRAS4 A to G327.3. Thus, the relative abundances of HCOOH to those of CH_3OH , CH_3CN , $\text{C}_2\text{H}_5\text{CN}$ and $\text{C}_2\text{H}_5\text{OH}$ seem to decrease with the protostellar luminosity.

We propose that the increase of $\text{CH}_3\text{OH}/\text{H}_2\text{CO}$ (as well as $\text{CH}_3\text{OH}/\text{HCOOH}$), $\text{CH}_3\text{CN}/\text{H}_2\text{CO}$, and $\text{C}_2\text{H}_5\text{CN}/\text{H}_2\text{CO}$ with stellar luminosity is likely due to differences in the grain mantle composition between low and massive star forming regions. Indeed, differences in the initial conditions (in particular gas density and dust temperature) are known to strongly affect surface chemistry. For example, Caselli et al. (1993) found that complex N-bearing species are more easily formed if the dust grain temperature (T_{dust}) is about 40 K, during the collapse phase. Although such temperature can be found in a significant fraction of a collapsing massive clump surrounding a massive young stellar object (Fontani et al. 2002), this is not the case for low mass cores. Therefore, the observed trend (at least for N-bearing species) is consistent with theoretical predictions. But Caselli et al. (1993) also found that at $T_{\text{dust}}\sim 40$ K, methanol is not efficiently formed on the surface because it requires the volatile H to stick on the grain surface (see also Charnley et al. 1992; van der Tak et al. 2000). Thus, the observed $\text{CH}_3\text{OH}/\text{H}_2\text{CO}$ increase with stellar luminosity is not well understood, unless another surface formation mechanism for methanol (besides the CO hydrogenation) becomes important in the warmer high mass clumps, e.g. $\text{OH}+\text{CH}_3$ (see also discussion in Pontoppidan et al. 2003). However, this conclusion is only based on 4 sources and has to be confirmed with a larger and more complete sample. Observational bias such as the different spatial scale for the different objects can contribute to give this trend if the spatial extension of the emission of the observed molecules is different.

In Fig. 7c, we compare only the N-bearing molecules. The $[\text{C}_2\text{H}_5\text{CN}]/[\text{CH}_3\text{CN}]$ ratio remains quite constant with a dispersion of about a factor <10 between all the sources. This uniform $[\text{C}_2\text{H}_5\text{CN}]/[\text{CH}_3\text{CN}]$ ratio suggesting that the chemistry of both compounds is linked. Indeed, these two molecules have a common parent species: C_2N (see e.g. Fig.7 in Caselli et al. 1993)

7. Conclusions: The chemistry of the IM hot core NGC 7129–FIRS 2

In this paper we present the first detection of an intermediate-mass hot core. Our interferometric observations towards FIRS 2 allow us to estimate a size of

650×900 AU and a mass of 2 M_{\odot} for the hot core associated with this IM object. The dimensions and mass of this IM hot core are intermediate between those measured in hot corinos ($r \sim 150$ AU, $M < 1 M_{\odot}$) and massive stars ($r \sim 3000$ AU, $M > 10 M_{\odot}$) and consequently one expects to find a differentiated chemistry in it.

Our interferometric observations of CH_3CN , CH_3OH , D_2CO and N_2D^+ provides information on the structure and chemistry of this object. While the CH_3CN emission arises mainly in the hot core, the CH_3OH emission has a component associated with the bipolar outflow. The CH_3CN abundance is $\sim 7.0 \cdot 10^{-9}$ in the hot core, which is about 3 orders of magnitude larger than in the cool envelope. The methanol abundance is enhanced ($> 3 \cdot 10^{-8}$ –a few 10^{-7}) in the hot core and the outflow components. However the rotation temperature is higher in the hot core than in the outflow revealing very different physical conditions, and probably a different CH_3OH desorption mechanism for the two components.

The doubly deuterated formaldehyde also presents enhanced abundances in the hot core. We estimate a $[\text{D}_2\text{CO}]/[\text{H}_2\text{CO}] \sim 0.14$, which is 4 orders of magnitude larger than the cosmic D abundance and similar to those found in pre-stellar clumps and low-mass protostars. The enhanced $[\text{D}_2\text{CO}]/[\text{H}_2\text{CO}]$ abundance in the hot core suggests that grain surface chemistry is responsible of the deuteration process of H_2CO . In contrast to the high deuteration degree of formaldehyde, we have not detected N_2D^+ in the hot core. This is consistent with the chemical scheme in which while the deuteration of H_2CO requires surface chemistry, the deuteration of N_2H^+ is a gas-phase process.

A large number of molecular lines have been detected in our interferometric spectra towards FIRS 2. Most of these lines are identified as belonging to deuterated (D_2CO , $c\text{-C}_3\text{D}$ and $c\text{-C}_3\text{HD}$), sulphuretted (^{13}CS , OCS) and complex O-/N-bearing species (HCOOH , $\text{C}_2\text{H}_5\text{OH}$, $\text{C}_2\text{H}_5\text{CN}$). Deuterated species whose deuteration requires surface chemistry, such as D_2CO , present enhanced abundances in the warm regions associated with low-mass protostars. Loinard et al. (2003) searched for the doubly deuterated form of formaldehyde (D_2CO) in a large sample of young stellar objects. D_2CO was detected in all low-mass protostars, with $[\text{D}_2\text{CO}]/[\text{H}_2\text{CO}]$ ratios of 2–40%. On the other hand, no detection was obtained towards more massive protostars (where $[\text{D}_2\text{CO}]/[\text{H}_2\text{CO}] < 0.5\%$). This is consistent with the results reported by Turner (1990) who detected D_2CO in Orion and measured $[\text{D}_2\text{CO}]/[\text{H}_2\text{CO}] \sim 0.003$. If the hot cores associated with massive stars are older or significantly denser than those surrounding low-mass objects, gas phase chemistry could have had the time to re-set the deuterium fractionation to values close to the cosmic D/H ratio. An alternative explanation is that the gas temperature of the material accreting high mass protostars is larger than 30 K (Fontani et al. 2002), so that the deuterium fractionation efficiency in the gas phase is strongly reduced already before the hot core phase

The sulphuretted and complex compounds are characteristic of hot cores in both the low-mass and the high-mass regimes. FIRS 2 is the first IM hot core detected thus far and presents a unique opportunity to study the link between the chemistry of hot corinos and massive hot cores. We have compared the abundances of complex molecules in FIRS 2 with those in hot corinos and the massive hot cores OMC1 and G327.3–0.6. Contrary to model predictions, we do not detect any dependence of the O-/N-complex molecules ratio on the protostellar luminosity. However, we detect differences between the behavior of the O-bearing species with the stellar luminosity. While H_2CO and HCOOH are more abundant in low luminosity sources, CH_3OH seems to be more abundant in massive objects. We propose that this could be due to a different mantle composition in the two kinds of region, caused by different physical conditions (mainly gas density and dust temperature) during the pre-stellar and accretion phase. However, this could also be due to other factors such as the different spatial scale of the observations or a possible contribution of the shocked gas associated with the bipolar outflow to the emission of these molecules. Differences in the hot core ages and/or cloud initial conditions could also produce these differences. The detection and detailed study of more intermediate-mass hot cores are necessary to establish firm conclusions.

Acknowledgements. This work has been partially supported by the Spanish DGICYT under grant AYA2003-07584 and Spanish DGI/SEPCT under grant ESP2003-04957. PC acknowledges support from the MIUR grant “Dust and molecules in astrophysical environments”. We are also grateful to the anonymous referee for his/her fruitful comments.

References

- Bacmann, A., Lefloch, B., Ceccarelli, C., Steinacker, J., Castets, A., Loinard, L. 2003, *ApJ*, 585, L55
- Bachiller, R., & Perez Gutierrez, M. 1997, *ApJL*, 487, L93
- Bergin, E. A., Alves, J., Huard, T., Lada, C. J. 2002, *ApJ*, 570, L101
- Bottinelli, S., et al. 2004, *ApJL*, 615, 354
- Brown, P. D., Charnley, S. B., Millar, T. J. 1988, *MNRAS*, 231, 409
- Butner, H. M., Lada, E. A., & Loren, R. B. 1995, *ApJ*, 448, 207
- Caselli, P., Hasegawa, T. I., & Herbst, E. 1993, *ApJ*, 408, 548
- Caselli, P., Walmsley, C. M., Tafalla, M., Dore, L., Myers, P. C. 1999, *ApJ*, 523, L165
- Caselli, P., Walmsley, C. M., Zucconi, A., Tafalla, M., Dore, L., Myers, P. C. 2002, *ApJ*, 565, 331
- Caselli, P., Stantcheva, T., Shalabiea, O., Shematovich, V. I., Herbst, E. 2002b, *P&SS*, 50, 1257
- Caselli, P., van der Tak, F. F. S., Ceccarelli, C., Bacmann, A. 2003, *A&A*, 403, L37
- Cazaux, S., et al. 2003, *ApJ*, 593, L51
- Ceccarelli, C., Loinard, L., Castets, A., Tielens, A. G. G. M., & Caux, E. 2000, *A&A*, 357, L9
- Ceccarelli, C., Loinard, L., Castets, A., Tielens, A. G. G. M., Caux, E., Lefloch, B., & Vastel, C. 2001, *A&A*, 372, 998

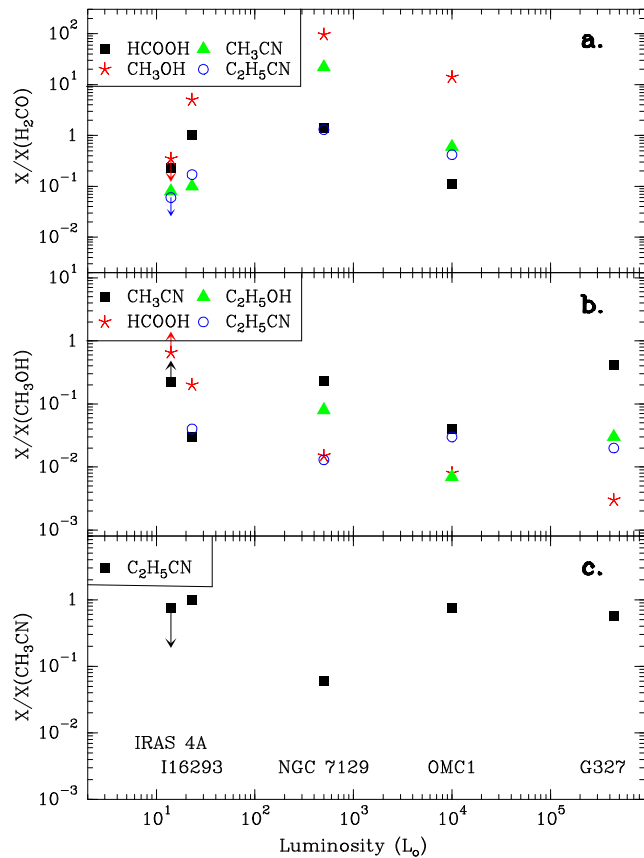


Fig. 7. Relative abundances of the complex O- and N-bearing molecules as a function of the protostellar luminosity for the objects listed in Table 3.

Ceccarelli, C., Vastel, C., Tielens, A. G. G. M., Castets, A., Boogert, A. C. A., Loinard, L., Caux, E. 2002, *A&A*, 381, L17

Crapsi, A., Caselli, P., Walmsley, C. M., Myers, P. C., Tafalla, M., Lee, C. W., Bourke, T. L. 2005, *ApJ*, 619, 379

Charnley, S. B., Tielens, A. G. G. M., Millar, T. J. 1992, *ApJ*, 399, L71

Charnley, S. B., Tielens, A. G. G. M., & Rodgers, S. D. 1997, *ApJL*, 482,

Fontani, F., Cesaroni, R., Caselli, P., Olmi, L. 2002, *A&A*, 389, 603, L203

Fuente, A., Martín-Pintado, J., Bachiller, R., Neri, R., & Palla, F. 1998, *A&A*, 334, 253

Fuente, A., Neri, R., Martín-Pintado, J., Bachiller, R., Rodríguez-Franco, A., & Palla, F. 2001, *A&A*, 366, 873 (Paper I)

Fuente, A., Martín-Pintado, J., Bachiller, R., Rodríguez-Franco, A., & Palla, F. 2002, *A&A*, 387, 977

Fuente, A., Rodríguez-Franco, A., Testi, L., Natta, A., Bachiller, R., & Neri, R. 2003, *ApJL*, 598, L39

Fuente, A., Rizzo, J.F., Caselli, P., Bachiller, R., Henkel, C. 2005, *A&A*, 433, 535 (Paper II)

Gibb, E., Nummelin, A., Irvine, W.M., Whittet, D.C.B., Bergman, P. 2000, *ApJ*, 545, 309

Hollis, J. M., Jewell, P. R., Lovas, F. J., Remijan, A., & Møllendal, H. 2004, *ApJL*, 610, L21

Horn, A., Møllendal, H., Sekiguchi, O., Uggerud, E., Roberts, H., Herbst, E., Viggiano, A. A., Fridgen, T. D. 2004, *ApJ*, 611, 605

Kramer, C., Alves, J., Lada, C. J., Lada, E. A., Sievers, A., Ungerechts, H., Walmsley, C. M. 1999, *A&A*, 342, 257

Loinard, L., et al. 2003, *SFCHEM 2002: Chemistry as a Diagnostic of Star Formation*, proceedings of a conference held August 21-23, 2002 at University of Waterloo, Waterloo, Ontario, Canada N2L 3G1. Edited by Charles L. Curry and Michel Fich. NRC Press, Ottawa, Canada, 2003, p. 351., 351

Maret, S., et al. 2004, *A&A*, 416, 577

Pickett, H.M., Poynter, R.L., Cohen, E.A., Delitsky, M.L., Pearson, J.D., Muller, H.S.P., 1998, *J. Quant. Spectrosc. & Rad. Transfer*, 60, 883

Pontoppidan, K. M., Dartois, E., van Dishoeck, E. F., Thi, W.-F., d'Hendecourt, L. 2003, *A&A*, 404, L17

Rodgers & Charnley 2001, *ApJ*, 546, 324

Roberts, H., Herbst, E., Millar, T. J. 2003, *ApJ*, 591, L41

Rodríguez, L. F., Loinard, L., D'Alessio, P., Wilner, D. J., & Ho, P. T. P. 2005, *ApJL*, 621, L133

Schoier, F.L., Jorgensen, J.K., van Dishoeck, E.F., & Blake, G.A. 2002, *A&A*, 390, 1001

Stantcheva, T., Herbst, E. 2003, *MNRAS*, 340, 983

Sutton, E.C., Peng, R., Danchi, W.C., Jaminet, P.A., Sandell, G., Russell, A.P.G. 1995, *ApJSS*, 97, 455

Tafalla, M., Myers, P. C., Caselli, P., Walmsley, C. M., Comito, C. 2002, *ApJ*, 569, 815

Tielens, A. G. G. M. 1983, *A&A*, 119, 177

Turner, B. E. 1990, *ApJL*, 362, L29

van der Tak, F. F. S., van Dishoeck, E. F., Caselli, P. 2000, *A&A*, 361, 327

Vastel, C., Phillips, T. G., Yoshida, H. 2004, *ApJ*, 606, L127

Viti, S., Collings, M. P., Dever, J. W., McCoustra, M. R. S., & Williams, D. A. 2004, *MNRAS*, 354, 1141

Wakelam, V., Caselli, P., Ceccarelli, C., Herbst, E., & Castets, A. 2004, *A&A*, 422, 159

Walmsley, C. M., Flower, D. R., Pineau des Forêts, G. 2004, *A&A*, 418, 1035

Watson, W. D. 1974, *ApJ*, 188, 35

Willacy, K., Langer, W. D., Velusamy, T. 1998, *ApJ*, 507, L171

Williams J.P., Bergin E.A., Caselli P., Myers P.C., Plume R., 1998, *ApJ* 503, 689

lli, C., Herbst, E., Castets, A., 2004, *A&A*, 422, 159

Wyrowski, F., Schilke, P., & Walmsley, C. M. 1999, *A&A*, 341, 882